ACS OMEGA

Open Access

http://pubs.acs.org/journal/acsodf

Article

Adsorption Mechanisms of CO_2 on Macroporous Ion-Exchange Resin Organic Amine Composite Materials by the Density Functional Theory

Yan Li, Xinmin Liu,* and Qingjie Guo

Cite This: *ACS Omega* 2024, 9, 17541−17550

Read Online

ACCESS | Metrics & More | Article Recommendations | Supporting Information

ABSTRACT: The adsorption mechanisms of CO_2 on macroporous cation exchange resin (MCER), D001 ion-exchange resin, and macroporous ion-exchange resin organic amine composite materials (MCER-DEA and D001-PEI) were studied by density functional theory (DFT). The adsorption energies and Mulliken atomic charges in the adsorption process were analyzed, indicating that CO_2 on MCER and D001 were physisorbed. The adsorption heat of the adsorption process of MCER-DEA and D001-PEI was calculated by the Monte Carlo method, and it was found that the adsorption process of CO_2 by MCER-DEA and D001-PEI was both physical adsorption and chemical adsorption. Besides, the chemical adsorption mechanism of CO_2 by MCER-DEA and D001-PEI was investigated by analyzing the free energy barrier and the Gibbs free energy change of the involved chemical reactions and the results showed that the free energy barrier required for MCER-DEA to generate zwitterion was 26.23 kcal/mol, which is 1.74 times that of D001-PEI (15.04 kcal/mol); meanwhile, the free energy barriers of the deprotonation process of zwitterions in MCER-DEA and D001-PEI were 16.23 and 9.89 kcal/mol, respectively, indicating that D001-PEI chemically adsorbs CO_2 and requires more energy than MCER-DEA chemical adsorption of CO_2. D001-PEI is more conducive to the chemical adsorption of CO_2. In addition, H_2O molecules were incorporated on the polymer models to study the influence of humidity on the CO_2 adsorption mechanism. The analysis revealed that the adsorption of CO_2 slowed under humid conditions.

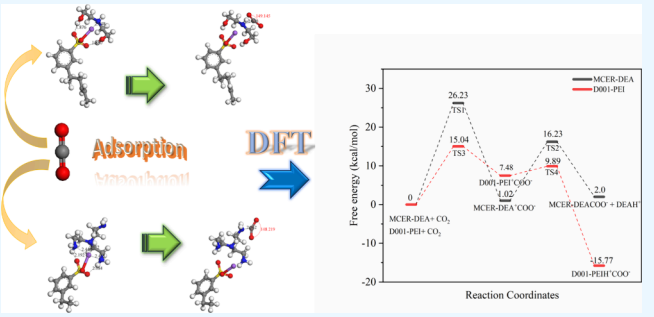

1. INTRODUCTION

In the last decades, combating the climate change caused by anthropogenic greenhouse gas (GHG) emissions has undoubtedly become one of the greatest challenges.[1] Our overreliance and uncontrolled exhaustive usage of fossil fuels as our primary energy source has led to an alarming rise in atmospheric carbon dioxide levels. The current CO_2 atmospheric concentration is near 420 ppm. Power generation is the highest contributor to the world's CO_2 emissions, with about 47% of the emissions generated in the electricity and heat sector and around 25% by the transport sector by 2021. The industrial sector (e.g., chemicals, petrochemicals, iron, and steel, aluminum, cement, or paper) generated about 18% of the total CO_2 emission.[2,3] The excessive emission of these GHGs is disastrous for the earth's climate, ecosystems, and species. The adverse consequences of climate warming are no longer just a potential threat but are very obvious and require immediate attention. Carbon dioxide is the main contributor to the greenhouse effect, and global CO_2 emissions are on the rise. Therefore, it is urgent to reduce CO_2 emissions from coal-fired power plants and tackle the rapid rise of the atmospheric CO_2 concentration.

A potential solution to curbing CO_2 emissions is carbon dioxide capture and storage (CCS). The separation of CO_2 can mainly be achieved by adsorption, physical and chemical absorption, cryogenic distillation, membrane separation, and other ways.[4] In the case of power plants, capturing combusted carbon dioxide through the absorption process is of greatest concern. However, current CO_2-capturing materials using the scrubbing method with aqueous amine solutions still face some serious defects, such as high energy consumption, severe equipment corrosion, and regeneration difficulties.[5,6] As a result, the use of porous materials for carbon dioxide capture and storage strategies has received increasing attention. A range of different porous solid adsorbents including zeolites,[7,8] silica,[9,10] porous carbon,[11,12] metal−organic frameworks (MOFs),[13,14] porous organic polymers (POPs),[15] and alkyldiamine-appended metal−organic frameworks (diamine-

Received: January 18, 2024
Revised: March 4, 2024
Accepted: March 28, 2024
Published: April 6, 2024

https://doi.org/10.1021/acsomega.4c00587
ACS Omega 2024, 9, 17541−17550

M_2(dobpdc))[16−19] has been proposed for CO_2 capture and storage. However, these porous materials are expensive. The advantages of a high surface area, good regeneration performance, and low cost make the adsorption of CO_2 by ion-exchange resins very promising.

For acidic CO_2 gas, impregnating the resin surface with organic amine has been exploited due to its high affinity for adsorbing CO_2 and trapping them into ammonium salts.[20] For example, Liu et al.[21,22] reported that diethanolamine (DEA) impregnated macroporous cation exchange resin (MCER) and polyethylenimine (PEI) impregnated ion-exchange resin (D001) show enhanced adsorption of CO_2 gas compared to the pure surface. They measured the properties using adsorption isotherms with empirical models such as pseudo-first-order, pseudo-second-order, Avrami, or Weber−Morris. Nevertheless, the understanding of the fundamental mechanism remains more or less unclear. Zhu et al.[23] applied molecular dynamics (MD) to analyze and establish the bituminous coal molecular model and investigated the adsorption behavior of coal in CO_2/N_2 mixed gas. However, their work was limited to studying the adsorption behavior of bituminous coal in different proportions of mixed gases based on Monte Carlo methods. Lima et al.[24] studied the adsorption of 15%CO_2/85%N_2 mixtures on monoethanolamine (MEA)-impregnated NaX zeolite based on the Monte Carlo method.

However, none of the above discuss the adsorption mechanism of CO_2 on different sorbents and the basic mechanism of the interaction between CO_2 and amine-impregnated resins remains unresolved at the molecular level. In this work, based on previous research in our laboratory,[21,22] the adsorption mechanisms of CO_2 on four types of macroporous ion-exchange resins (MCER, MCER-DEA, D001, and D001-PEI) were studied by DFT. The Materials Studio DMol3 module was used to obtain the optimized adsorption configurations. The adsorption energies and Mulliken atomic charges in the adsorption process were analyzed. The adsorption heat of MCER-DEA and D001-PEI adsorption processes was calculated using the Monte Carlo method, and the diffusion coefficients of 15% CO_2/85% N_2 mixed components in MCER-DEA and D001-PEI simulation boxes were further calculated through MD. Furthermore, the free energy barriers and the Gibbs free energy of the chemical adsorption process were calculated by the transition state search and optimization. H_2O molecules were incorporated into the polymer models to study the influence of the humidity on the CO_2 adsorption mechanism.

2. SIMULATION DETAILS

2.1. Mechanical Quantum. *2.1.1. Models.* In order to represent the interaction process between CO_2 molecules and macroporous cation exchange resin, the simplified models were established to represent the two macroporous cation exchange resins (MCER and D001) and the two amine solutions (polyethylenimine and DEA) in Figure 1, respectively. For convenience, the C atoms, H atoms, N atoms, O atoms, S atoms, and Na atoms are represented in gray, white, blue, red, yellow, and purple, respectively. A polybutadiene-polystyrene monomer model containing the sodium sulfonate group was constructed to represent MCER, and the optimized resin model is shown in Figure 1a. The D001 model was obtained by replacing polybutadiene-polystyrene with polystyrene molecules, and its optimal atomic structure is displayed in Figure 1b. The ethylenimine monomer was constructed to simulate PEI, and its optimal structure is displayed in Figure 1c. The optimal structure of DEA is displayed in Figure 1d. The optimal structure of the CO_2 molecule is shown in Figure 1e, where the C═O bond length is 1.61 Å, which is similar to the experimental data.

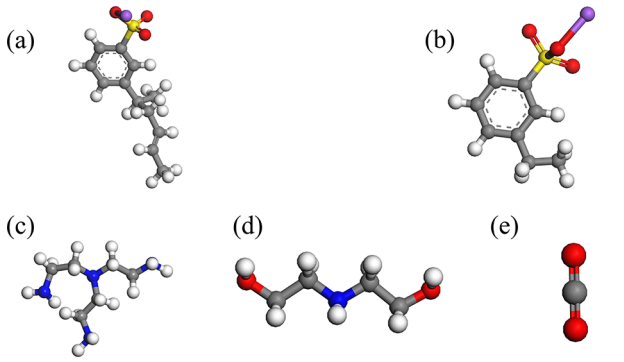

Figure 1. Optimized structures of the most stable state for (a) MCER, (b) D001, (c) PEI, (d) DEA, and (e) CO_2. The yellow, purple, red, blue, gray, and white spheres represent S, Na, O, N, C, and H, respectively.

2.1.2. Methods. Material quantum properties were calculated using the DMol3 module, and graphical displays were created with Materials Studio (MS) 2017. The structure was optimized by using the geometric optimization task provided by the DMol3 module. Then, the Mulliken analysis was used to calculate atomic charges using the analysis section of the DMol3 module.[25] In addition, in theoretical analysis, the Perdew−Burke−Ernzerhof (PBE) function under the generalized gradient approximation (GGA) was used to describe the exchange-correlation energy.[26] The double numerical plus polarization (DNP) basis set with the 3.5 Å basis file was selected in consideration of valence electrons, which is comparable to the split-valence double-ζ 6-31G** in size, but it is more accurate than the Gaussian basis sets of the same size.[27] The van der Waals (vdW) interactions, using the DFT-D method of Grimme, was considered in all of the calculations.[28] A Fermi smearing of 0.005 Ha and a global orbital cutoff of 5.2 Å were employed. The adsorption energy, E_{ads}, is used to evaluate the adsorption effect between the adsorbate and adsorbent and defined as follows:

$$E_{ads} = E_{(adsorbent+adsorbate)} - E_{(adsorbent)} - E_{(adsorbate)} \quad (1)$$

where $E_{(adsorbent+adsorbate)}$, $E_{(adsorbent)}$, and $E_{(adsorbate)}$ are the total energy of the system, adsorbent, and the adsorbate (kcal/mol), respectively. The more negative the adsorption energy, the stronger the bond between the adsorbent and the adsorbate.

To accurately understand the mechanism of adsorption of the CO_2 gas molecules on macroporous ion-exchange resin organic amine composite materials, density functional theory-based electronic structure calculations and meta-dynamics method-based first-principles molecular dynamics (FPMD) simulations were employed to analyze the energetics and free energy profile of the involved chemical reactions. Vibrational frequency calculations were carried out for the optimized structures; all of the optimized structures were confirmed with no imaginary frequency except one imaginary frequency for the transition state. When defining atomic pairs, the appropriate reactants and products involved in each mechanism are considered; accordingly, a 3D trajectory file representing a preview of the reaction path is generated for each mechanism

https://doi.org/10.1021/acsomega.4c00587
ACS Omega 2024, 9, 17541−17550

with the Reaction Preview tool of the Materials Studio software. These 3D trajectory files are then used as inputs, using linear synchronous transit, and quadratic synchronous transit (LST/QST) calculations, which are minimized by the conjugate gradient[29] in the transition state search tool in DMol3. Then, the particular mode is selected to perform transition state optimization to verify whether the obtained geometry is indeed a transition state. Activation free energy (E_a) and Gibbs free energy change (ΔG) were calculated using eqs 2 and 3:[29,30]

$$E_a = E_{(\text{transition state})} - E_{(\text{reactant})} \quad (2)$$

$$\Delta G = E_{(\text{product})} - E_{(\text{reactant})} \quad (3)$$

where E_{reactant}, $E_{\text{transition state}}$, and E_{product} represent the energies of the reactant, transition state, and product (kcal/mol), respectively.

2.2. Molecular Dynamics. *2.2.1. Construction of Simulation Boxes.* An MD approach was used to simulate the diffusion of 15% CO_2/85% N_2 mixture components on MCER-30%DEA and D001−30%PEI. First, the homopolymer part of the construction module was used to create MCER and D001 polymer chains with tactical (isotropic), chain number (1), and chain length (10), with the chain length modified to 8 for the PEI polymer chain. It is crucial to use appropriate repeating units in the simulations of all polymers, as the accuracy and precision of the simulation depend on it. Through geometric optimization of the Forcite module, structural optimization was conducted for the DEA compound as well as the MCER, D001, and PEI polymer models, with a maximum iteration of 500 to achieve the actual equilibrium state. The geometric optimization energy of the structure is shown in Figure S1. As shown in the figure, the initial energy of MCER (1374.1 kcal/mol), D001 (1581.8 kcal/mol), DEA (52 kcal/mol), and PEI (500.5 kcal/mol) structures has been decreased to −216.4, −191.7, 11, and 194.1 kcal/mol, respectively. From the graph, it can be seen that the energy level optimization of the system was successful, reaching the lowest value of the system. According to energy values, PEI and MCER have the lowest and highest stabilities.

Simulation boxes with specific composition ratios were developed using the Amorphous Cell module, where the weight fraction of organic amines in the solid amine adsorbent was 30%, as shown in Figure 2. The amorphous models were then geometrically optimized to exclude undesirable interactions and achieve the lowest energy state. The Compass II[23] force field in the Materials Studio software strengthened support for polymer systems compared with other force fields and can be applied to adsorption simulations of various polymers constructed in this article. Accordingly, in MD simulations, the Compass II force field was always used for Force Field in Energy. The equilibrium of the simulation boxes is typically measured by their density, temperature, and energy. Therefore, the stable or fluctuating behaviors of the MCER-30% DEA and D001−30% PEI simulation boxes in terms of density, temperature, and energy indicate convergence to an equilibrium state. To determine the equilibrium density of the simulation boxes, NPT-MD simulations were conducted at 1×10^{-4} GPa, 298 K, and a total simulation time of 500 ps. The thermodynamic stability of the simulation boxes was then examined through energy analysis from NVT-MD analysis conducted under conditions of 298 K, 1×10^{-4} GPa, and 500 ps. Figure S2 presents a schematic illustration of the equilibrium behavior of the simulation boxes based on temperature, density, and energy fluctuations of the MCER-30% DEA and D001−30% PEI materials. As shown in Figure S2a, the temperatures of both materials reached equilibrium after 500 ps. The density values of MCER-30% DEA fluctuated between 1.05 and 1.10 (g/cm^3), with the density of the simulation box reaching equilibrium after 500 ps, as seen in Figure S2b. The density values of D001−30% PEI fluctuated between 1.05 and 1.15 (g/cm^3), with the density of the simulation box reaching equilibrium after 500 ps. Figure S2c,d represents the energy fluctuations of total energy, potential energy, kinetic energy, and nonbond energy calculated for MCER-30% DEA and D001−30% PEI simulation boxes, as well as the average energy of all simulation boxes. It is evident from the energy fluctuations of the simulation boxes that all energies reached equilibrium within 500 ps. The parameters of the simulated amorphous cells for MCER-30% DEA and D001−30% PEI at 298 K are listed in Table 1.

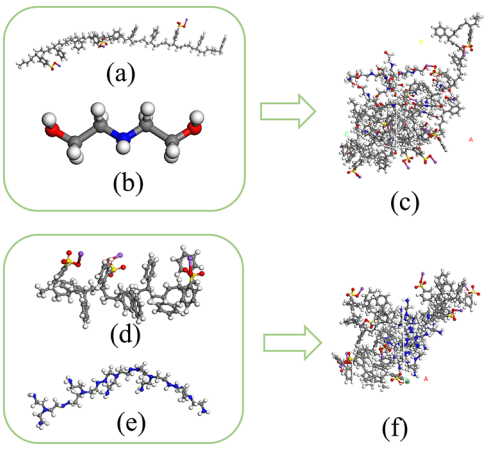

Figure 2. Simulation models: (a) MCER, (b) DEA, (c) MCER-30% DEA, (d) D001, (e) PEI, and (f) D001−30% PEI.

Table 1. Parameters of MCER-30% DEA and D001-30% PEI Simulation Boxes at 0.1 mPa and 298 K

	cell length (Å)	cutoff distance (Å)	volume (Å^3)	density (g/cm^3)
MCER-30% DEA	23.8	12.5	12,406.8	1.08
D001−30% PEI	21.0	12.5	9313.5	1.11

2.2.2. Methods. The adsorption behavior of 15% CO_2/85% N_2 mixed components on MCER-30% DEA and D001−30% PEI materials was studied using the Sorption module. The simulation steps are as follows: The Monte Carlo method was used for calculation, the task was set as fixed pressure; CO_2 partial pressure was set to 15 kPa, and N_2 partial pressure was set to 85 kPa; the electrostatic field was set to Ewald & Group, and vdW interaction was calculated as atom based. The adsorption heat was calculated as follows:

$$Q_{st} = RT\left[\frac{d(\ln P)}{d(\ln T)}\right] \quad (4)$$

After using the grand canonical ensemble:

$$Q_{st} = RT - G \quad (5)$$

https://doi.org/10.1021/acsomega.4c00587
ACS Omega 2024, 9, 17541−17550

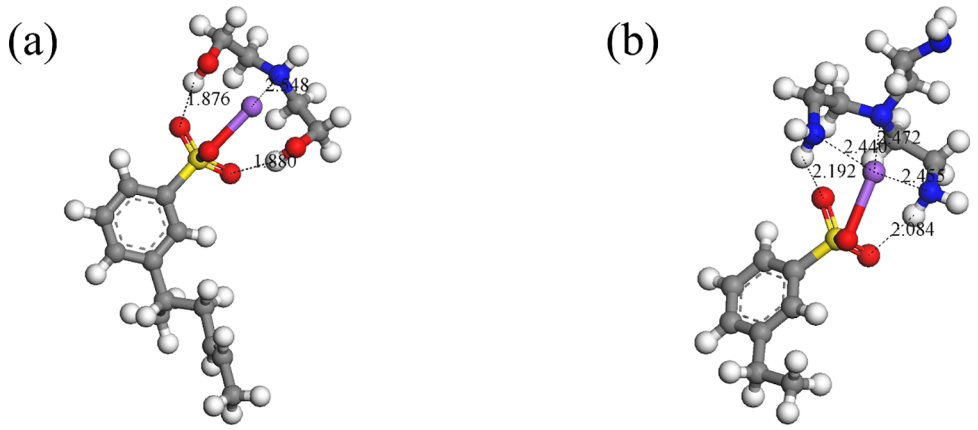

Figure 3. Optimized structures of the most stable configurations for (a) DEA-loaded MCER and (b) PEI-loaded D001. All bond distances are in Å.

$$G = \langle E \rangle - \mu_{\text{intra}} \langle N \rangle \quad (6)$$

wherein Q_{st} is the adsorption heat (kcal/mol), R is the universal gas constant (2.03×10^{-3} kcal·mol^{-1}·k^{-1}), T is the temperature (K), P is the absolute equilibrium pressure (Torr), E is the total energy (kcal/mol), μ represents the chemical potential (kcal/mol), and N represents the number of particles.[31]

The most stable low-energy adsorption configuration was extracted based on the fixed pressure calculation in the Sorption module, and the diffusion coefficient was further calculated. The low-energy adsorption configuration was geometrically optimized in the Forcite module to achieve a stable energy state of the models. Then, MD simulations were performed using isobaric isotherms (NPT) to estimate the equilibrium density of the mixture. The system was compressed and decompressed until the density remained constant with a pressure of 0.1 MPa, a temperature of 298 K, a time step of 1 fs, and a total simulation time of 500 ps. In addition, the Forcite module isothermal−isochoric (NVT) ensemble was applied to achieve simulated box equilibria at 0.1 MPa and 298 K, with a total simulation time of 500 ps and a time step of 1 fs. A final MD run was performed on a hybrid simulation box using the Forcite module's microcanonical (NVE) ensemble, with a total simulation time of 500 ps. After the completion of the dynamic simulations, the trajectory distribution of CO_2 and N_2 molecules moving inside the MCER-30% DEA and D001−30% PEI boxes can be obtained. The mean square displacement curves (MSD) can be obtained through analysis. Meanwhile, the diffusion coefficient (D) can be calculated by using the Einstein method (eq 7), and the calculation can be simplified to eq 8.

$$D = \frac{1}{6N} \frac{\mathrm{d}}{\mathrm{d}t} \lim_{t \to \infty} \sum_{k=1}^{N} [|r_i(t) - r_i(0)|^2] \quad (7)$$

$$D = k/6 \quad (8)$$

In the formula, N is the number of diffusing atoms in the system, $[|r_i(t) - r_i(0)|^2]$ denotes the MSD, t is the time (ps), and k denotes the slope of the MSD curve.

3. RESULTS AND DISCUSSION

3.1. Loading of Organic Amines on Macroporous Ion-Exchange Resins. The MCER-DEA model was built by connecting one MCER monomer and one DEA monomer, and the D001-PEI model was built by connecting one D001 monomer and one PEI monomer (as shown in Figure 3). Then, the geometric models of the two polymers were geometrically optimized to make the energy of the models reach a stable state and the optimized molecular configuration was reversed and distorted. To ensure that the optimization of the adsorption system converged to the global minimum on the corresponding energy surface, the Adsorption Locator module was used to determine the low-energy adsorption sites by conducting a Monte Carlo search on the configuration space of the substrate−adsorbate system. Then, the DMol3 module was used for geometric optimization to obtain the most stable adsorption configurations of MCER-DEA and D001-PEI. The results are shown in Figure 3, and their corresponding adsorption properties are summarized in Table 2.

Table 2. Adsorption Energies (E_{ads}) of the Adsorption Configurations and the Mulliken Charges (Q) Transferred between the Organic Amines and the Macroporous Ion-Exchange Resins

	E_{ads} (kcal/mol)	Q (e)
MCER-DEA	−60.19	0.001
D001-PEI	−50.11	0.004

A DFT study demonstrated that positive electric "Na" of MCER interacts with the negative electric "N" of DEA while the double-bonded oxygen atoms of the $-SO_3Na$ group are very electronegative, and they strongly interact with the electropositive "H" atoms of the −OH group in DEA, thus resulting in the formation of a hydrogen-bonded structure, as shown in Figure 3. The positive electric "Na" of D001 interacts with the negative electric "N" of PEI, and the double-bonded oxygen atoms of the $-SO_3Na$ group and the electropositive "H" atoms of the $-NH_2$ group in PEI interact strongly to form a hydrogen-bonded structure. From Figure 3, it can also be seen that the distance between the double-bond oxygen atoms of MCER and the "H" atoms of the −OH group in DEA is 1.88 Å whereas the distance between the double-bond oxygen atoms of D001 and the "H" atoms in $-NH_2$ of PEI is 2.08 and 2.19 Å, indicating that the hydrogen bond strength formed between MCER and DEA is greater than that of D001-PEI.

The adsorption energies and transferred Mulliken charges between the organic amines and the macroporous ion-exchange resins are listed in Table 2. The adsorption energy of MCER-DEA is −60.19 kcal/mol, while the adsorption

https://doi.org/10.1021/acsomega.4c00587
ACS Omega 2024, 9, 17541−17550

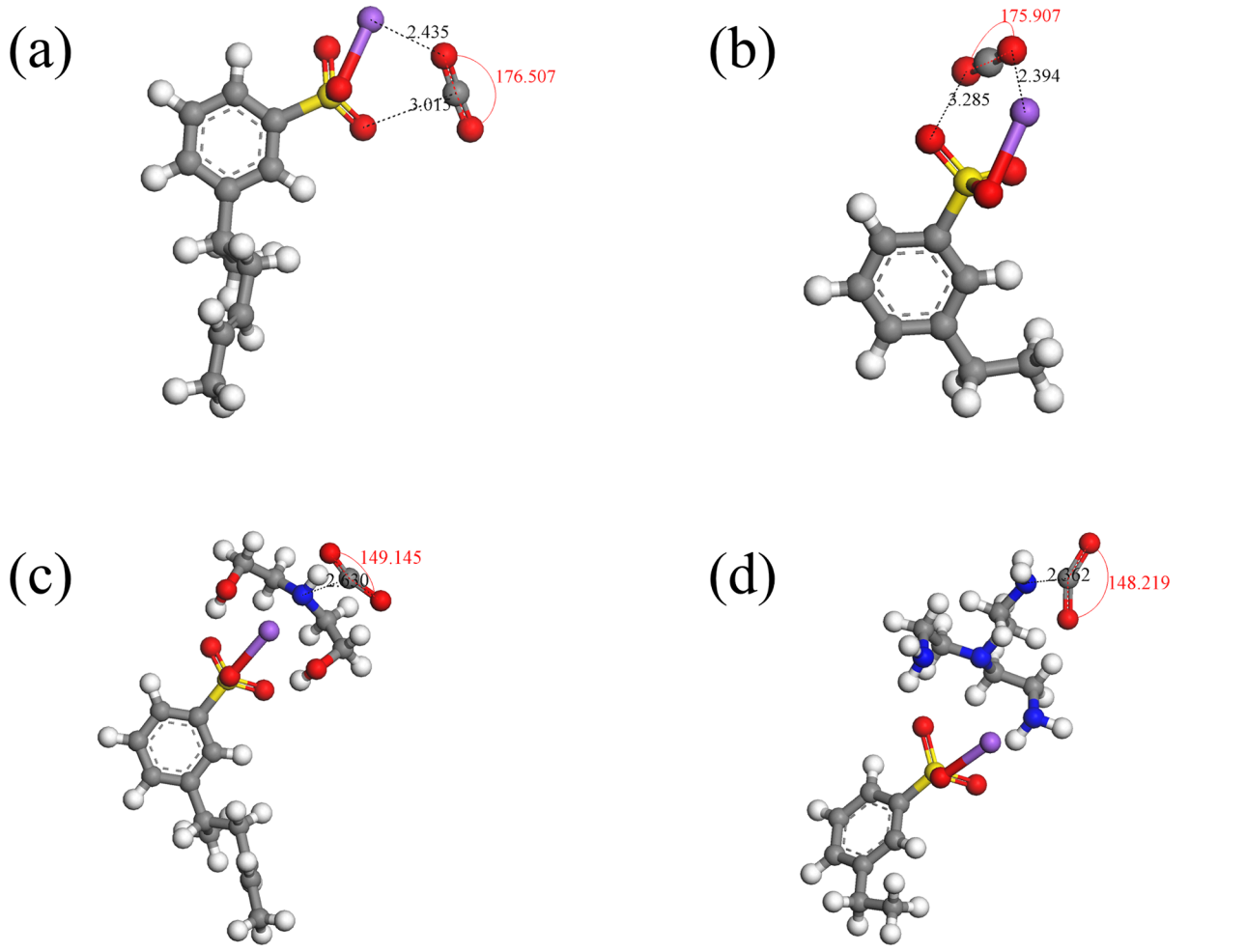

Figure 4. Optimized structures of the most stable configurations for the CO_2 on (a) MCER, (b) D001, (c) MCER-DEA, and (d) D001-PEI.

energy of D001-PEI is −50.11 kcal/mol. This further illustrates that the hydrogen bonds formed between MCER-DEA are more stable than those of D001-PEI. A positive value of the change in Mulliken atomic charges indicates a loss of electrons, and a negative value indicates the accumulation of electrons.[28] From Table 2, it can be found that DEA adsorbed on MCER has a positive charge of 0.001 e and PEI adsorbed on D001 has a positive charge of 0.004 e. This demonstrates that the charge distribution can be changed by the loading of organic amines onto macroporous ion-exchange resins and organic amines provide their electrons to the surface of ion-exchange resin materials.

3.2. Adsorption of CO_2 on Different Adsorbed Materials. The CO_2 molecule was placed on the models to study the interactions between CO_2 and the four adsorbed materials, as illustrated in Figure 4. The adsorption energies and the transferred Mulliken charges of CO_2 molecules on different adsorption materials are listed in Table 3. The adsorption energy between CO_2 and MCER is −8.13 kcal/mol, which is higher than that of D001 (−7.49 kcal/mol), mainly because the electronegative "O" of CO_2 interacts more strongly with the electropositive "Na" of MCER than with D001. The results indicate that the adsorption of CO_2 on MCER and D001 is simple physical adsorption, and this is consistent with the experimental data that the adsorption capacity of CO_2 on MCER (1.87 mmol/g) is greater than that of CO_2 on D001 (1.07 mmol/g).[21,22] The adsorption energies

Table 3. Adsorption Energies (E_{ads}) of the Adsorption Configurations, and the Mulliken Charges (Q) Transferred between the CO_2 Molecules and the Adsorbing Materials

	E_{ads} (kcal/mol)	Q (e)	O−C−O bond angles (°)
MCER	−8.13	0.001	176.5
D001	−7.49	−0.001	175.9
MCER-DEA	−17.59	0.104	149.1
D001-PEI	−18.64	0.235	148.2

of the CO_2 molecules in MCER-DEA and D001-PEI are −17.59 and −18.64 kcal/mol, respectively. These values are close to B_{38} fullerene (−15.96 kcal/mol)[32] and Ni-decorated InN (−15.22 kcal/mol)[33] but greater than the results of C_9N_7 (−6.46 kcal/mol)[34] and Se-doped graphene (−5.01 kcal/mol).[35] Considering that the E_{ads} of CO_2 on a high-performance adsorbent are preferably between −9.78 kcal/mol and −19.57 kcal/mol,[32] the MCER-DEA and D001-PEI are thus effective CO_2 storage adsorbents.

According to the analysis of the amounts of Mulliken charge transfer, it can be found that almost all the charge change values are positive, which demonstrates that the CO_2 molecules act like the donors, donating their electrons to the surface of the adsorption materials.[28] Due to this weak physical adsorption, a negligible charge of about 0.001 e is transferred from CO_2 to MCER. The Mulliken charge transfer from MCER-DEA and D001-PEI to CO_2 molecules is about 0.104

https://doi.org/10.1021/acsomega.4c00587
ACS Omega 2024, 9, 17541−17550

and 0.235 e. The results indicate that the charge distribution can be changed by the adsorption of the CO_2 molecule on MCER-DEA and D001-PEI, and the adsorption process may involve chemical adsorption. When CO_2 is adsorbed on MCER and D001, there is little structural transformation. However, when CO_2 molecules were adsorbed on MCER-DEA and D001-PEI, the structural deformation of the CO_2 molecules occurs; the O−C−O bond angles are 149.1 and 148.2°, respectively. These results show that CO_2 was physisorbed on MCER and D001, while it was chemisorbed on MCER-DEA and D001-PEI.

3.3. Analyses of MD Simulation Results. Adsorption heat (Q_{st}) refers to the thermal effect generated by the adsorption reaction of the adsorbent materials during the adsorption process, which is one of the important parameters characterizing the adsorption capacity of the adsorbent materials. Q_{st} < 20 kJ/mol (1 Ha = 2565.5 kJ/mol = 627.51 kcal/mol) indicates physical adsorption, while Q_{st} > 60 kJ/mol indicates chemical adsorption.[36] The adsorption heats of CO_2 in MCER-30% DEA and D001−30% PEI virtual simulation boxes were determined using the MS software metropolis algorithm and Sorption module. The isosteric adsorption heat of MCER-30% DEA and D001−30% PEI under different CO_2 partial pressure is plotted in Figure 5. By comparison of the isosteric adsorption heats of different adsorption materials, it can be concluded that the adsorption methods of MCER-30% DEA and D001−30% PEI for CO_2 are both physical and chemical adsorption, with chemical adsorption being the main method. Moreover, D001−30% PEI has stronger chemical adsorption capacity than MCER-30% DEA. Liu et al.[22] found that when the adsorption amount is less than 2 mmol/g, both physical and chemical adsorptions occur simultaneously, with chemical adsorption being the main method. When the adsorption amount exceeds 2.0 mmol/g, as the amino active sites gradually become occupied, they mainly undergo physical adsorption and reach adsorption equilibrium.

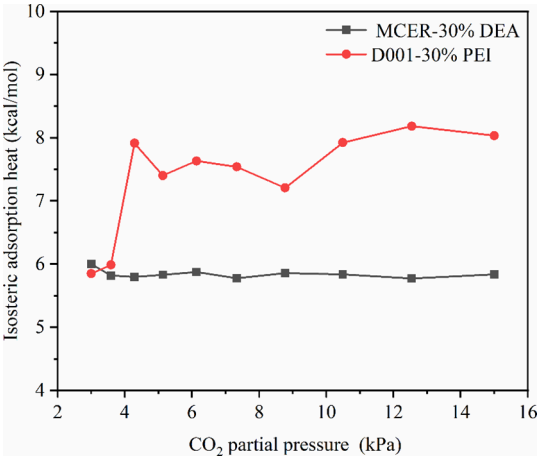

Figure 5. Simulated isosteric adsorption heat of MCER-30% DEA and D001−30% PEI with CO_2 partial pressure at 333 K.

The diffusion coefficients of the 15% CO_2/85% N_2 mixture components in MCER-30% DEA and D001−30% PEI were calculated. Based on the values of MSD plotted in Figure 6 as a function of time, a linear fit was performed to obtain the slope of the straight line, and the diffusion coefficients of the gases through the MCER-30% DEA and D001−30% PEI simulation boxes were calculated using eq 8. The results are listed in Table 4. In the MCER-30% DEA and D001−30% PEI simulation boxes, the diffusion coefficients of CO_2 are higher than those of N_2. The high diffusion coefficient of CO_2 is due to its smaller kinetic diameter (3.3 Å) compared with N_2 (3.88 Å).[37] Generally, by incorporation of organic amines into the polymer matrix, solid chemical interactions can be generated between the amine groups on the MCER-30% DEA and D001−30% PEI surfaces and CO_2 molecules, thereby increasing the diffusion of CO_2 gas.

Table 4. Diffusion Coefficients of 15% CO_2/85% N_2 Mixed in MCER-30% DEA and D001-30% PEI

adsorbent	adsorbate	$y = b*x + a$	R^2	diffusivity coefficient (10^{-5} cm^2/s)
MCER-30% DEA	CO_2	$y = 1.11x + 11.87$	0.9984	1.85
	N_2	$y = 0.71x + 11.47$	0.9850	1.18
D001−30% PEI	CO_2	$y = 1.65x + 11.20$	0.9786	2.75
	N_2	$y = 0.87x + 12.23$	0.9970	1.45

3.4. Mechanism of Reaction of CO_2 by MCER-DEA and D001-PEI. To further investigate the reaction mechanisms of CO_2 capture by MCER-DEA and D001-PEI, the Transition State (TS) Search and TS Optimization function of the DMol3 module were used to calculate the reaction pathways and free energy changes. According to previous reports, the adsorption of CO_2 by solid amine adsorption materials is mainly adsorbed by chemical reaction between amino groups and CO_2,

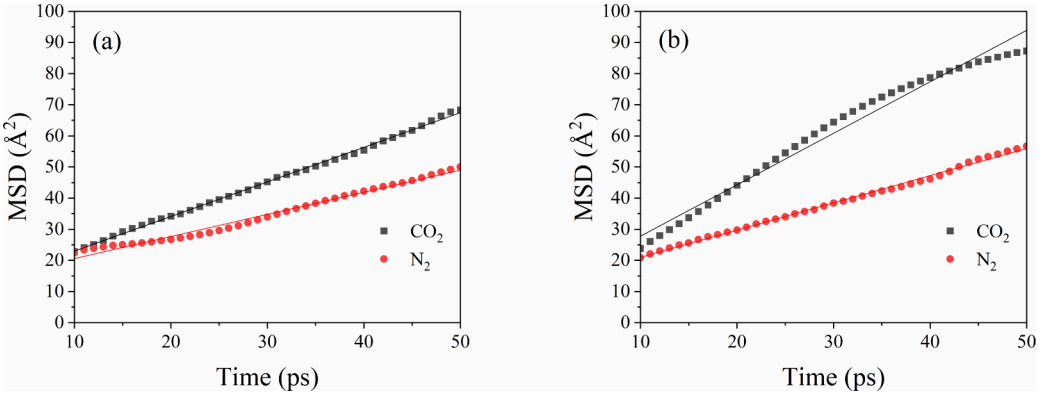

Figure 6. MSD curves of 15% CO_2/85% N_2 mixed in (a) MCER-30% DEA and (b) D001−30% PEI.

https://doi.org/10.1021/acsomega.4c00587
ACS Omega 2024, 9, 17541−17550

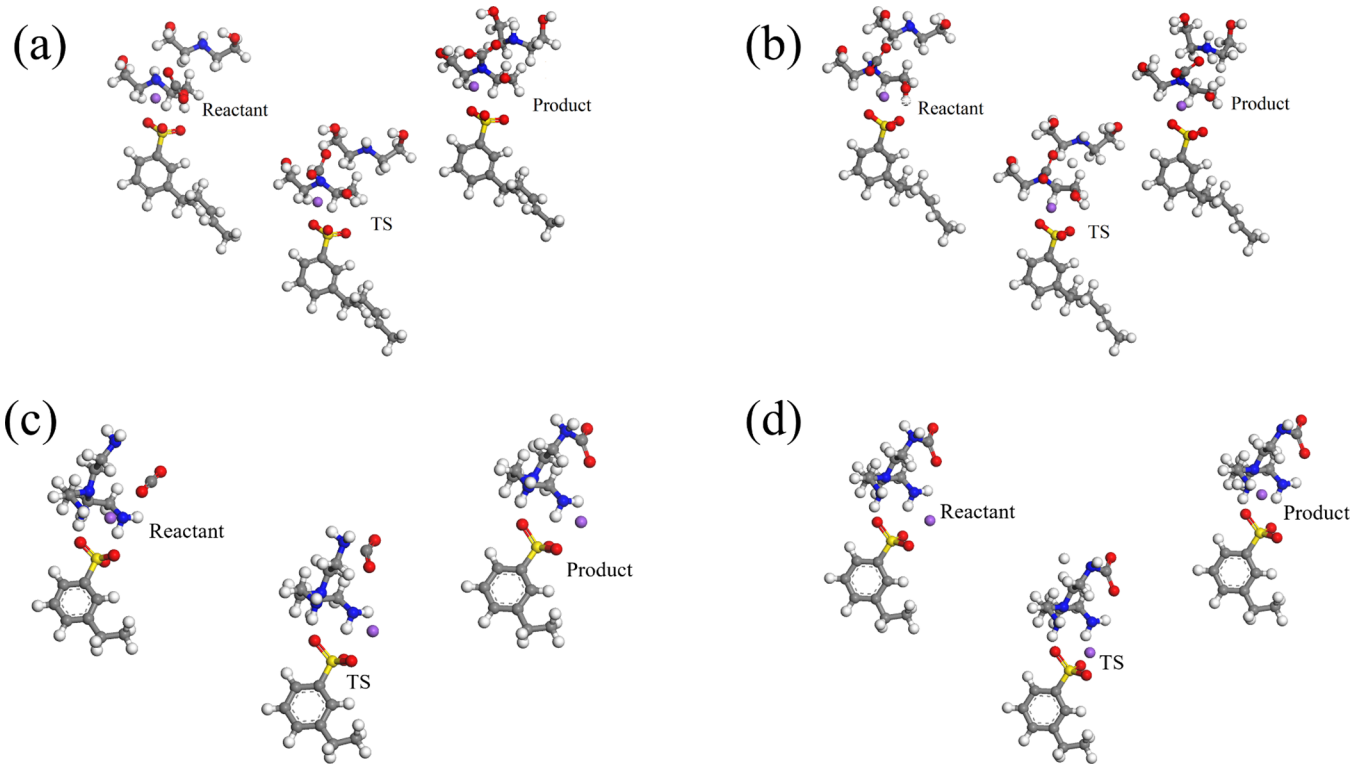

Figure 7. Detailed geometries of reactants, transition states, and products during the process of zwitterion generation (a) MCER-DEA surface and (c) D001-PEI surface and during the process of zwitterion deprotonation (b) MCER-DEA surface and (d) D001-PEI surface.

following the zwitterionic mechanism,[38] in which amino groups first combine with CO_2 to form zwitterions and then are deprotonated to form carbamates. Therefore, two reaction pathways were set up and are expressed as eq 9-12. Pathways I-1 and I-2 represented the reaction of MCER-DEA and CO_2, and pathways II-1 and II-2 represented the reaction of D001-PEI and CO_2.

$$\mathrm{I-1: MCER-DEA + CO2 \rightarrow MCER-DEA^{+}COO^{-}} \quad (9)$$

$$\mathrm{I-2: MCER-DEA^{+}COO^{-} + DEA \rightarrow MCER-DEACOO^{-} + DEAH^{+}} \quad (10)$$

$$\mathrm{II-1: D001-PEI + CO2 \rightarrow D001-PEI + COO-} \quad (11)$$

$$\mathrm{II-2: D001-PEI + COO- \rightarrow D001-PEIH + COO-} \quad (12)$$

The transition state of the CO_2 adsorption process is shown in Figure 7. Figure 7a,c shows the detailed geometries of reactants, transition states, and products during the process of zwitterion generation on MCER-DEA and D001-PEI, respectively. Figure 7b,d shows the detailed geometries of reactants, transition states, and products during the process of zwitterion deprotonation on MCER-DEA and D001-PEI, respectively. Then, the activation free energy and the free energy changes under the two reaction pathways are shown in Figure 8. In both pathways, the activation free energy involved in zwitterions is higher than that of deprotonation of zwitterions, which means that the formation of zwitterions is the rate-determining step of the reaction. This is consistent with the previously reported results.[30,38] The free energy barrier required for MCER-DEA to generate the zwitterion is

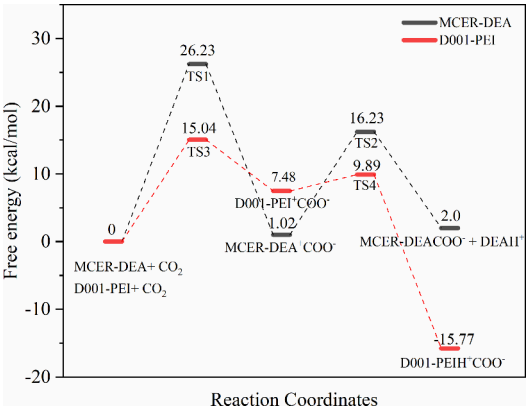

Figure 8. Schematic of free energy surfaces for CO_2 absorption in MCER-DEA and D001-PEI.

26.23 kcal/mol, which is 1.74 times that of D001-PEI (15.04 kcal/mol). The Gibbs free energy changes for the generation of zwitterions by MCER-DEA and D001-PEI are 1.02 and 7.48 kcal/mol, respectively, indicating that D001-PEI has a higher reactivity with CO_2. The free energy barriers of the deprotonation process of zwitterions in MCER-DEA and D001-PEI are 16.23 and 9.89 kcal/mol, and the Gibbs free energy changes of the deprotonation process of zwitterions in MCER-DEA and D001-PEI are 2.0 and −15.77 kcal/mol, respectively, indicating that pathway II-2 is more prone to occur than pathway I-2 and D001-PEI has a stronger ability to accept protons. The results show that MCER-DEA chemically adsorbs CO_2 requiring more energy than D001-PEI and that D001-PEI is more conducive to the chemical adsorption of CO_2. This is consistent with the results of CO_2 adsorption experiment: The adsorption amount of D001-PEI to CO_2 (4.0

https://doi.org/10.1021/acsomega.4c00587
ACS Omega 2024, 9, 17541−17550

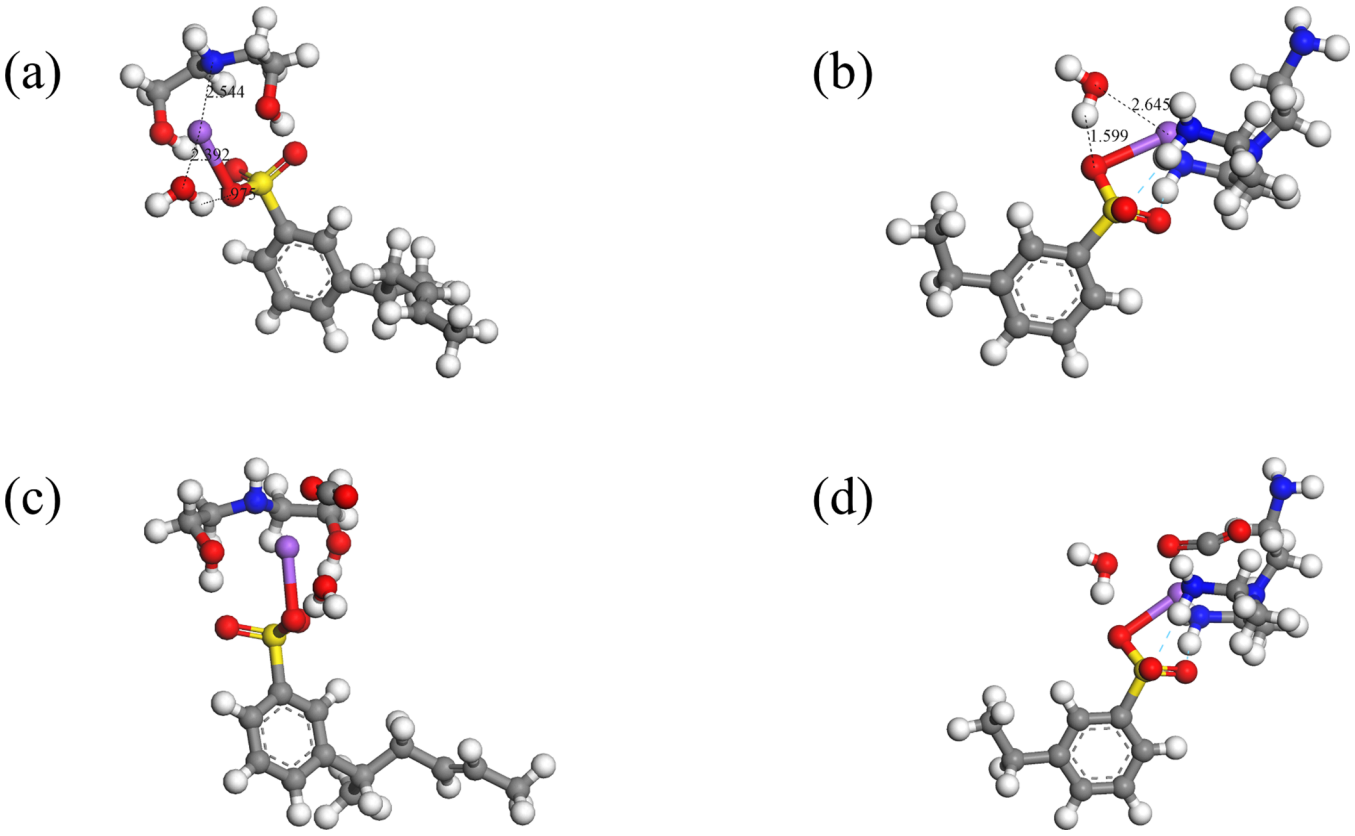

Figure 9. Optimized structures of the most stable configurations for the H_2O on (a) MCER-DEA and (b) D001-PEI and optimized structures of the most stable configurations for the CO_2 on aqueous materials (c) MCER-DEA and (d) D001-PEI.

mmol/g) is much greater than that of MCER-DEA (2.87 mmol/g), D001-PEI reaches adsorption equilibrium in 24 min, while MCER-DEA reaches adsorption equilibrium in 40 min, and the adsorption rate of CO_2 by MCER-DEA is slower.[21,22]

3.5. The Effect of Humidity on the Adsorption Mechanism of CO_2. A H_2O molecule was incorporated on polymer models to study the influence of humidity on the adsorption mechanism of CO_2, as shown in Figure 9. Under the conditions of H_2O and no H_2O, the adsorption energies of the CO_2 molecules on the adsorbing materials are listed in Table 5. MCER-DEA and D001-PEI are hydrophilic materials

Table 5. Adsorption Energies of Different Molecules on the MCER-DEA and D001-PEI Models

surface type	CO_2 (kcal/mol)	H_2O (kcal/mol)	CO_2 with H_2O (kcal/mol)
MCER-DEA	−4.61	−12.47	−3.85
D001-PEI	−5.53	−16.44	−5.0

because macroporous adsorption resins contain sulfonic acid groups that form hydrogen bonds with the "H" of H_2O molecules while the positive electric "Na" of the $-SO_3Na$ group interacts with the negative electric "O" of H_2O. The adsorption energy of a H_2O molecule on different solid adsorption materials was calculated, and D001-PEI was the more hydrophilic material with a larger adsorption energy of −16.44 kcal/mol. When H_2O molecules are present on the surface, the CO_2 adsorption energy of all of the polymer models decreased slightly. This is because H_2O molecules occupy the adsorption site of CO_2 molecules on macroporous adsorption resins. In addition, water can also induce the leaching of amine compounds. This means that the adsorption rate of CO_2 molecules slows under humid conditions. As a result, MCER-DEA and D001-PEI could be negative for the effect of humidity on CO_2 adsorption.

4. CONCLUSIONS

The adsorption mechanisms of CO_2 on MCER, D001, MCER-DEA, and D001-PEI were investigated by DFT. Physical adsorption occurred in the adsorption of CO_2 by the four types of solid adsorption materials. The adsorption of CO_2 on MCER and D001 was weak physisorption, in accordance with the vdW interactions between the microporous ion-exchange resins and CO_2. In addition, the adsorption heat generated by the adsorption materials during the adsorption process was calculated and the adsorption heat of MCER-DEA and D001-PEI was >20 kJ/mol, indicating that both physical adsorption and chemical adsorption occurred during the CO_2 adsorption process of MCER-DEA and D001-PEI. The activation free energy of the chemical adsorption process was calculated by the transition state search and optimization. It was found that MCER-DEA chemically adsorbs CO_2 requiring more energy than D001-PEI and that D001-PEI was more conducive to the chemical adsorption of CO_2. Most interestingly, it was found that the humidity slightly degrades the adsorption capability of the solid adsorption materials for CO_2. This was ascribed to H_2O molecules occupying the adsorption site of CO_2 molecules on macroporous adsorption resins. Therefore, the presence of H_2O should be avoided as much as possible during the CO_2 adsorption process. This study could help us better understand the CO_2 adsorption mechanism of macroporous

https://doi.org/10.1021/acsomega.4c00587
ACS Omega 2024, 9, 17541−17550

ion-exchange resin organic amine composite materials at the molecular level.

■ ASSOCIATED CONTENT

Supporting Information

The Supporting Information is available free of charge at https://pubs.acs.org/doi/10.1021/acsomega.4c00587.

The calculated lattice parameters and unit cell volumes for MCER, D001, D001-PEI, MCER-DEA, MCER-CO_2, D001-CO_2, D001-PEI-CO_2, and MCER-DEA-CO_2; geometry optimization energy analysis graphs of MCER, D001, DEA, and PEI structures; schematic diagram of the equilibrium calculation of the periodic box of the adsorption materials; and the optimized geometry structures and corresponding coordinate files (PDF)

■ AUTHOR INFORMATION

Corresponding Author

Xinmin Liu − *State Key Laboratory Base of Eco-Chemical Engineering in College of Chemical Engineering, Qingdao University of Science and Technology, Qingdao 266042, China;* orcid.org/0000-0002-5155-5829; Email: lxm220@qust.edu.cn

Authors

Yan Li − *State Key Laboratory Base of Eco-Chemical Engineering in College of Chemical Engineering, Qingdao University of Science and Technology, Qingdao 266042, China*

Qingjie Guo − *State Key Laboratory Base of Eco-Chemical Engineering in College of Chemical Engineering, Qingdao University of Science and Technology, Qingdao 266042, China*

Complete contact information is available at: https://pubs.acs.org/10.1021/acsomega.4c00587

Notes

The authors declare no competing financial interest.

■ ACKNOWLEDGMENTS

This work was supported by the Foundation of State Key Laboratory of High-efficiency Utilization of Coal and Green Chemical Engineering (2021-K20) and the National Natural Science Foundation of China (21706141).

■ REFERENCES

(1) Garcia, J. A.; Villen-Guzman, M.; Rodriguez-Maroto, J. M.; Paz-Garcia, J. M. Technical Analysis of CO_2 Capture Pathways and Technologies. *J. Environ. Chem. Eng.* **2022**, *10* (5), No. 108470.

(2) Liu, W.; Teng, L.; Rohani, S.; Qin, Z.; Zhao, B.; Xu, C. C.; Ren, S.; Liu, Q.; Liang, B. CO_2 Mineral Carbonation Using Industrial Solid Wastes: A Review of Recent Developments. *Chem. Eng. J.* **2021**, *416*, No. 129093.

(3) Ren, S.; Aldahri, T.; Liu, W.; Liang, B. CO_2 Mineral Sequestration by Using Blast Furnace Slag: From Batch to Continuous Experiments. *Energy* **2021**, *214*, No. 118975.

(4) Parekh, A.; Chaturvedi, G.; Dutta, A. Sustainability Analyses of CO_2 Sequestration and CO2 Utilization as Competing Options for Mitigating CO_2 Emissions. *Sustain. Energy Technol. Assess.* **2023**, *55*, No. 102942.

(5) Zhao, Y.; Bian, Y.; Li, H.; Guo, H.; Shen, S.; Han, J.; Guo, D. A Comparative Study of Aqueous Potassium Lysinate and Aqueous monoethanolamine for Postcombustion CO_2 Capture. *Energy Fuels* **2017**, *31* (12), 14033−14044.

(6) Meng, F.; Meng, Y.; Ju, T.; Han, S.; Lin, L.; Jiang, J. Research Progress of Aqueous Amine Solution for CO_2 Capture: A Review. *Renew. Sustain. Energy Rev.* **2022**, *168*, No. 112902.

(7) Aquino, T. F. D.; Estevam, S. T.; Viola, V. O.; Marques, C. R. M.; Zancan, F. L.; Vasconcelos, L. B.; Riella, H. G.; Pires, M. J. R.; Morales-Ospino, R.; Torres, A. E. B.; Bastos-Neto, M.; Cavalcante, C. L. CO_2 Adsorption Capacity of Zeolites Synthesized from Coal Fly Ashes. *Fuel* **2020**, *276*, No. 118143.

(8) Choi, H. J.; Min, J. G.; Ahn, S. H.; Shin, J.; Hong, S. B.; Radhakrishnan, S.; Chandran, C. V.; Bell, R. G.; Breynaert, E.; Kirschhock, C. E. A. Framework Flexibility-Driven CO_2 Adsorption on a Zeolite. *Mater. Horiz.* **2020**, *7* (6), 1528−1532.

(9) Jung, W.; Lee, K. S. Isotherm and Kinetics Modeling of Simultaneous CO_2 and H_2O Adsorption on an Amine-Functionalized Solid Sorbent. *J. Nat. Gas Sci. Eng.* **2020**, *84*, 103489.

(10) Ravutsov, M.; Mitrev, Y.; Shestakova, P.; Lazarova, H.; Simeonov, S.; Popova, M. CO_2 Adsorption on Modified Mesoporous Silicas: The Role of the Adsorption Sites. *Nanomaterials* **2021**, *11* (11), 2831.

(11) Hao, J.; Wang, X.; Wang, Y.; Lai, X.; Guo, Q.; Zhao, J.; Yang, Y.; Li, Y. Hierarchical Structure N, O-Co-Doped Porous Carbon/Carbon Nanotube Composite Derived from Coal for Supercapacitors and CO_2 Capture. *Nanoscale Adv.* **2020**, *2* (2), 878−887.

(12) Yan, H.; Zhang, G.; Xu, Y.; Zhang, Q.; Liu, J.; Li, G.; Zhao, Y.; Wang, Y.; Zhang, Y. High CO_2 Adsorption on Amine-Functionalized Improved Macro-/Mesoporous Multimodal Pore Silica. *Fuel* **2022**, *315*, No. 123195.

(13) Kang, J. H.; Yoon, T.-U.; Kim, S.-Y.; Kim, M.-B.; Kim, H.-J.; Yang, H.-C.; Bae, Y.-S. Extraordinarily Selective Adsorption of CO_2 over N_2 in a Polyethyleneimine-Impregnated NU-1000 Material. *Microporous Mesoporous Mater.* **2019**, *281*, 84−91.

(14) Ghahramaninezhad, M.; Mohajer, F.; Niknam Shahrak, M. Improved CO_2 Capture Performances of ZIF-90 through Sequential Reduction and Lithiation Reactions to Form a Hard/Hard Structure. *Front. Chem. Sci. Eng.* **2020**, *14* (3), 425−435.

(15) Han, J.; Du, Z.; Zou, W.; Li, H.; Zhang, C. Moisture-Responsive Hydrogel Impregnated in Porous Polymer Foam as CO_2 Adsorbent in High-Humidity Flue Gas. *Ind. Eng. Chem. Res.* **2015**, *54* (31), 7623−7631.

(16) Zhang, H.; Yang, L.-M.; Ganz, E. Adsorption Properties and Microscopic Mechanism of CO_2 Capture in 1,1-Dimethyl-1,2-Ethylenediamine-Grafted Metal−Organic Frameworks. *ACS Appl. Mater. Interfaces* **2020**, *12* (16), 18533−18540.

(17) Zhang, H.; Yang, L.-M.; Pan, H.; Ganz, E. Atomistic Level Mechanism of CO_2 Adsorption in *N* -Ethylethylenediamine-Functionalized M_2 (Dobpdc) Metal−Organic Frameworks. *Cryst. Growth Des.* **2020**, *20* (10), 6337−6345.

(18) Zhang, H.; Shang, C.; Yang, L.-M.; Ganz, E. Elucidation of the Underlying Mechanism of CO_2 Capture by Ethylenediamine-Functionalized M_2 (Dobpdc) (M = Mg, Sc−Zn). *Inorg. Chem.* **2020**, *59* (22), 16665−16671.

(19) Zhang, H.; Yang, L.-M.; Ganz, E. Unveiling the Molecular Mechanism of CO_2 Capture in *N* -Methylethylenediamine-Grafted M_2 (Dobpdc). *ACS Sustain. Chem. Eng.* **2020**, *8* (38), 14616−14626.

(20) Singh, G.; Lee, J.; Karakoti, A.; Bahadur, R.; Yi, J.; Zhao, D.; AlBahily, K.; Vinu, A. Emerging Trends in Porous Materials for CO2 Capture and Conversion. *Chem. Soc. Rev.* **2020**, *49* (13), 4360−4404.

(21) Liu, X.; Niu, Y.; Huang, Y.; Qiu, X.; Guo, Q. Preparation of macroporous Ion-Exchange Resin Organic Amine Composite Material by Using Waste Plastics and Its Application in CO_2 Capture. *Environ. Technol.* **2023**, *44* (6), 886−895.

(22) Liu, X.; Qiu, X.; Sun, X.; Mei, L.; Wang, L.; Guo, Q. Preparation and Kinetic Study of Organic Amine-loaded Ion-exchange Resin as CO_2 Adsorbents. *Environ. Prog. Sustain. Energy* **2021**, *40* (1), No. e13476, DOI: 10.1002/ep.13476.

(23) Zhu, H.; Guo, S.; Xie, Y.; Zhao, H. Molecular Simulation and Experimental Studies on CO_2 and N_2 Adsorption to Bituminous Coal. *Environ. Sci. Pollut. Res.* **2021**, *28* (13), 15673−15686.
(24) Lima, A. E. O.; Gomes, V. A. M.; Lucena, S. M. P. Universidade Federal do Ceará, Brasil. Theoretical study of CO_2: N_2 adsorption in faujasite impregnated with monoethanolamine. *Braz. J. Chem. Eng.* **2015**, *32* (3), 663−669.
(25) Delley, B. From Molecules to Solids with the DMol3 Approach. *J. Chem. Phys.* **2000**, *113* (18), 7756−7764.
(26) Chun, H.; Kang, J.; Han, B. First Principles Computational Study on the Adsorption Mechanism of Organic Methyl Iodide Gas on Triethylenediamine Impregnated Activated Carbon. *Phys. Chem. Chem. Phys.* **2016**, *18* (47), 32050−32056.
(27) Han, L.; Liu, K.; Wang, M.; Wang, K.; Fang, L.; Chen, H.; Zhou, J.; Lu, X. Mussel-Inspired Adhesive and Conductive Hydrogel with Long-Lasting Moisture and Extreme Temperature Tolerance. *Adv. Funct. Mater.* **2018**, *28* (3), 1704195.
(28) Li, K.; Li, N.; Yan, N.; Wang, T.; Zhang, Y.; Song, Q.; Li, H. Adsorption of Small Hydrocarbons on Pristine, N-Doped and Vacancy Graphene by DFT Study. *Appl. Surf. Sci.* **2020**, *515*, No. 146028.
(29) Ma, M.; Liu, Y.; Chen, Y.; Jing, G.; Lv, B.; Zhou, Z.; Zhang, S. Regulatory Mechanism of a Novel Non-Aqueous Absorbent for CO_2 Capture Using 2-Amino-2-Methyl-1-Propanol Low Viscosity and Energy Efficient. *J. CO2 Util.* **2023**, *67*, No. 102277.
(30) Gao, X.; Li, X.; Cheng, S.; Lv, B.; Jing, G.; Zhou, Z. A Novel Solid−Liquid 'Phase Controllable' Biphasic Amine Absorbent for CO_2 Capture. *Chem. Eng. J.* **2022**, *430*, No. 132932.
(31) Yuqing, H.; Liu, X.; Hu, X.; Guo, Q. Treatment of Phenolic Wastewater by Anaerobic Fluidized Bed Microbial Fuel Cell Filled with Polyaniline−macroporous Adsorption Resin as Multifunctional Carrier. *Can. J. Chem. Eng.* **2023**, *101* (10), 5530−5541.
(32) Esrafili, M. D.; Abolghasemzadeh, S. Carbon Dioxide Storage and Separation Using All-Boron B38 Fullerene: DFT Calculations. *Chem. Phys. Lett.* **2022**, *790*, No. 139361.
(33) Tao, L.; Dastan, D.; Wang, W.; Poldorn, P.; Meng, X.; Wu, M.; Zhao, H.; Zhang, H.; Li, L.; An, B. Metal-Decorated InN Monolayer Senses N_2 against CO_2. *ACS Appl. Mater. Interfaces* **2023**, *15* (9), 12534−12544.
(34) Liu, Z.; Li, X.; Shi, D.; Guo, F.; Zhao, G.; Hei, Y.; Xiao, Y.; Zhang, X.; Peng, Y. L.; Sun, W. Superior Selective CO_2 Adsorption and Separation over N_2 and CH_4 of Porous Carbon Nitride Nanosheets: Insights from GCMC and DFT Simulations. *Langmuir* **2023**, *39* (18), 6613−6622.
(35) Gholizadeh, R.; Yu, Y.-X. N_2O + CO Reaction over Si- and Se-Doped Graphenes: An Ab Initio DFT Study. *Appl. Surf. Sci.* **2015**, *357*, 1187−1195.
(36) Huang, H. Y.; Yang, R. T.; Chinn, D.; Munson, C. L. Amine-Grafted MCM-48 and Silica Xerogel as Superior Sorbents for Acidic Gas Removal from Natural Gas. *Ind. Eng. Chem. Res.* **2003**, *42* (12), 2427−2433.
(37) Bernardo, P.; Jansen, J. C.; Bazzarelli, F.; Tasselli, F.; Fuoco, A.; Friess, K.; Izák, P.; Jarmarová, V.; Kačírková, M.; Clarizia, G. Gas Transport Properties of Pebax®/Room Temperature Ionic Liquid Gel Membranes. *Sep. Purif. Technol.* **2012**, *97*, 73−82.
(38) Xie, H. B.; Zhou, Y.; Zhang, Y.; Johnson, J. K. Reaction Mechanism of monoethanolamine with CO_2 in Aqueous Solution from Molecular Modeling. *J. Phys. Chem. A* **2010**, *114* (43), 1184411852.

https://doi.org/10.1021/acsomega.4c00587
ACS Omega 2024, 9, 17541−17550